J|A|C|S ARTICLES

Published on Web 03/22/2010

An STM Study of the pH Dependent Redox Activity of a Two-Dimensional Hydrogen Bonding Porphyrin Network at an Electrochemical Interface

Qunhui Yuan, Yangjun Xing, and Eric Borguet*

Department of Chemistry, Temple University, 1901 North 13th Street, Philadelphia, Pennsylvania 19122

Received September 1, 2009; E-mail: eborguet@temple.edu

Abstract: Studying electron transfer reactions of porphyrin molecules is important for a wide range of applications including biology, molecular devices, artificial photosynthesis, information storage, and fuel cells. It is known that porphyrins adsorbed in a self-assembled monolayer at an electrochemical interface may lose their electrochemical activity. However, the mechanism of the suppressed electrochemical activity is not clear. In this article, the electrochemical behavior of the two-dimensional network structures of 5,10,15,20-tetrakis(4-carboxylphenyl)-21*H*,23*H*-porphyrin (TCPP) molecules, formed via intermolecular hydrogen bonding on Au(111), was investigated by electrochemical scanning tunneling microscopy (EC-STM). Three types of domains, including a square network with molecules trapped inside, square packing, and hexagonal close-packing structures have been observed under various pH conditions. The difference in STM contrast between oxidized and reduced TCPP allows the slow electrochemical reduction of adsorbed TCPP to be visualized by STM. For the first time, the pH dependent reduction of porphyrins was imaged by EC-STM, revealing the mechanism of porphyrin slow reduction at electrochemical interfaces. TCPP reduction can be accelerated either by tuning the working electrode potential to a more negative value or by lowering the H^+ concentration. A redox reaction model was proposed based on the pH dependent reduction of TCPP to elucidate the fundamental aspects of porphyrin redox reactions.

Introduction

Their unique electronic properties and reactivity enable porphyrins to have a wide range of applications from biology, molecular devices, artificial photosynthesis, information storage, to fuel cells.[1−9] Because of their importance in fundamental and applied studies, the formation and characterization of ordered porphyrin adlayers have been extensively studied in the last two decades by scanning tunneling microscopy (STM) under various conditions, including ultra high vacuum (UHV), air, and electrochemical environments.[10−44]

Most early studies of porphyrin assemblies were performed under UHV. For example, Gimzewski's group showed that the self-assembled structures of Cu-tetrakis(3,5-di-*tert*-butylphenyl)porphyrin (CuTBPP) strongly depend on the substrate materials (Cu, Au, Ag).[10,11] Intermolecular interactions, e.g., dipole−dipole interactions or intermolecular hydrogen bonding, can lead to a variety of supramolecular structures, such as trimers, tetramers, and 1D wire-like arrays, as observed by

(1) Balzani, V. *Electron Transfer in Chemistry*; Wiley-VCH: New York: 2001; Vol. 3.
(2) Forrest, S. R. *Chem. Rev.* **1997**, *97*, 1793–1896.
(3) Dolphin, V. D. *The Porphyrins*; Academic Press: New York, 1979.
(4) Fukuzumi, S. *Org. Biomol. Chem.* **2003**, *1*, 609–620.
(5) Guldi, D. M. *Chem. Soc. Rev.* **2002**, *31*, 22–36.
(6) Imahori, H.; Mori, Y.; Matano, Y. *J. Photochem. Photobiol., C* **2003**, *4*, 51–83.
(7) Jortner, J.; Ratner, M. *Molecular Electronics*; IUPAC: Oxford, 1997.
(8) Yeager, E. *Electrochim. Acta* **1984**, *29*, 1527–1537.
(9) Collman, J. P.; Boulatov, R.; Sunderland, C. J.; Fu, L. *Chem. Rev.* **2004**, *104*, 561–588.
(10) Jung, T. A.; Schlittler, R. R.; Gimzewski, J. K.; Tang, H.; Joachim, C. *Science* **1996**, *271*, 181–184.
(11) Jung, T. A.; Schlittler, R. R.; Gimzewski, J. K. *Nature* **1997**, *386*, 696–698.
(12) Yokoyama, T.; Yokoyama, S.; Kamikado, T.; Okuno, Y.; Mashiko, S. *Nature* **2001**, *413*, 619–621.
(13) Yokoyama, T.; Kamikado, T.; Yokoyama, S.; Mashiko, S. *J. Chem. Phys.* **2004**, *121*, 11993–11997.
(14) Scudiero, L.; Barlow, D. E.; Hipps, K. W. *J. Phys. Chem. B* **2000**, *104*, 11899–11905.
(15) Scudiero, L.; Barlow, D. E.; Mazur, U.; Hipps, K. W. *J. Am. Chem. Soc.* **2001**, *123*, 4073–4080.
(16) Bonifazi, D.; Spillmann, H.; Kiebele, A.; de Wild, M.; Seiler, P.; Cheng, F. Y.; Guntherodt, H. J.; Jung, T.; Diederich, F. *Angew. Chem., Int. Ed.* **2004**, *43*, 4759–4763.
(17) Li, W. S.; Kim, K. S.; Jiang, D. L.; Tanaka, H.; Kawai, T.; Kwon, J. H.; Kim, D.; Aida, T. *J. Am. Chem. Soc.* **2006**, *128*, 10527–10532.
(18) Sugiura, K.; Tanaka, H.; Matsumoto, T.; Kawai, T.; Sakata, Y. *Chem. Lett.* **1999**, 1193–1194.
(19) Kato, A.; Sugiura, K.; Miyasaka, H.; Tanaka, H.; Kawai, T.; Sugimoto, M.; Yamashita, M. *Chem. Lett.* **2004**, *33*, 578–579.
(20) Shoji, O.; Tanaka, H.; Kawai, T.; Kobuke, Y. *J. Am. Chem. Soc.* **2005**, *127*, 8598–8599.
(21) Lei, S. B.; Wang, C.; Yin, S. X.; Wang, H. N.; Xi, F.; Liu, H. W.; Xu, B.; Wan, L. J.; Bai, C. L. *J. Phys. Chem. B* **2001**, *105*, 10838–10841.
(22) Qiu, X. H.; Wang, C.; Zeng, Q. D.; Xu, B.; Yin, S. X.; Wang, H. N.; Xu, S. D.; Bai, C. L. *J. Am. Chem. Soc.* **2000**, *122*, 5550–5556.
(23) Wang, H. N.; Wang, C.; Zeng, Q. D.; Xu, S. D.; Yin, S. X.; Xu, B.; Bai, C. L. *Surf. Interface Anal.* **2001**, *32*, 266−270.
(24) Zhou, Y. S.; Wang, B.; Zhu, M. Z.; Hou, J. G. *Chem. Phys. Lett.* **2005**, *403*, 140–145.
(25) Scudiero, L.; Hipps, K. W. *J. Phys. Chem. C* **2007**, *111*, 17516–17520.
(26) Lipkowski, J.; Stolberg, L.; Yang, D. F.; Pettinger, B.; Mirwald, S.; Henglein, F.; Kolb, D. M. *Electrochimica Acta* **1994**, *39*, 1045−1056.

10.1021/ja907397u

Yokoyama et al. using CN or COOH group substituted TBPP molecules.[12,13] The Hipps group, combining theoretical calculations and STM observations under UHV of sublimed layers of one or multiple kinds of metal-coordinated porphyrins on surfaces, found that the metal ion valence configuration, especially the status of the dz^2 orbital, strongly affects the observed tunneling contrast in STM images.[14,15] Recently, several examples of supramolecular architectures formed by assembly of fullerenes and porphyrins have been studied under UHV. For instance, Bonifazi et al. reported a correlated arrangement between fullerene in the second layer and porphyrin arrays underneath.[16] The self-assembly of coordinated porphyrin complexes[17] and multiporphyrin supramolecular arrays have been imaged by STM.[18−20]

There are several reports about the adlayer structures of porphyrin under ambient conditions. Bai and Wan et al. reported a two-dimensional hydrogen bonding network of 5,10,15,20-tetrakis(4-carboxylphenyl)-21*H*,23*H*-porphyrin (TCPP) on HOPG using stearic acid lamellae as a stabilizing barrier.[21] They also demonstrated the stabilizing effect of linear alkanes on the assembly of a planar organic molecule by using an alkylated porphyrin to achieve highly stable structures on inert surfaces, e.g., HOPG.[22,23] Hou's group reported a coexistence of "face-on" and "edge-on" stacking structures on the HOPG surface by using the porphyrin derivative 5-hydroxyphenyl-10,15,20-tris(4-dodecyloxyphenyl)porphyrinatozinc(II) (ZnDPPOH).[24] It is claimed that the van der Waals forces and the hydrogen bonds, as well as $\pi-\pi$ interactions between the conjugated porphyrin cores, together contribute to the stability of the monolayer.[24] Recently, Scudiero and Hipps reported a controlled manipulation of self-organized Ni(II)-octaethylporphyrin (NiOEP) monolayer on the HOPG surface. A novel record of the growth of the damaged film created by STM has been introduced.[25]

STM has also been extensively used in investigating the structures of porphyrin adlayers in electrochemical environments.[26−44] At the electrode−solution interface, the molecular self-assembly process depends on the balance between molecule−molecule, molecule−substrate, and molecule−solvent interactions.[42] Compared to the vacuum−solid or gas−solid interfaces, tuning the working electrode potential provides a convenient way to adjust the molecule−substrate interaction and surface mobility of molecules at electrolyte−solid interfaces. In addition, the electrochemical environment enables the investigation of the unique electronic and chemical properties of porphyrins, such as interfacial electron transfer, coordination, and electrocatalysis.[34−36] Itaya's group reported a series of experiments on highly ordered porphyrin arrays including single, multiple component, and fullerene−porphyrin supramolecular assemblies.[27−29,31,33,34,36−38] For example, they found that iodine- or sulfur-modified metal surfaces provide weakened adsorbate−substrate binding which results in ordered porphyrin arrays instead of disordered structures as observed on bare metal surfaces.[27−33] Interesting electrocatalytical enhancements of O_2 reduction at the single molecule level on porphyrin-modified Au interfaces has also been discovered.[34−36,39] Tao et al. reported a series of adlayer structures formed by iron(III) protoporphyrin(FePP), zinc(II) protoporphyrin(ZnPP), and protoporphyrin IX(PP) in aqueous solutions.[40,41] Recently, potential controlled manipulation of surface mobility and redox activity of a metal-free, water-soluble tetrapyridylporphyrin (TPyP) on Au(111) was demonstrated in acid solutions.[42−44]

Among these studies, only a small number of papers addressed the interfacial electron transfer of porphyrin molecules although it is an essential step for electronics, electrochemistry, and solar-energy conversion.[38,41,43,44] For example, Itaya et al. reported the observation of ZnTPP reduction at the Au(111)/electrolyte interface.[37] The imaging of redox reactions of TPyP with single molecule resolution using electrochemical STM (EC-STM) was also reported.[43] It was found that the reduction of adsorbed TPyP is orders of magnitude slower than that of solution-phase TPyP.[43,44] However, our understanding of electrochemical dynamics and redox properties of adsorbed porphyrins is still limited, especially the details of the mechanism of porphyrin electrochemical reactions on surfaces.

It was suggested that the slow reduction of TPyP is due to a rate-limiting, protonation step on the nitrogen atoms at the porphyrin core, which, in principle, should depend on the pH of the solution.[43,45,46] However, the pH dependence with single molecule resolution afforded by EC-STM has not been investigated previously. Herein, we report the results of experiments designed to systematically study the reduction dynamics of porphyrins to understand how the concentration of H^+ affects the reduction behavior of TCPP at Au(111)/electrolyte interfaces. In addition, we show that the ability to distinguish oxidized and reduced porphrins by EC-STM is not limited to TPyP. We chose TCPP because we hypothesized that the redox reaction previously observed in TPyP[43] should be observed in other porphyrins that have the same porphyrin core structure. We found that (1) TCPP molecules form three types of arrays, reflecting various ways for intermolecular hydrogen bonds to stabilize molecular networks. (2) Absorbed TCPP molecules undergo a slow reduction process similar to the reported TPyP redox reaction.[43] (3) Lower $[H^+]$ accelerates the reduction rate

(27) Itaya, K. *Prog. Surf. Sci.* **1998**, *58*, 121–247.
(28) Kunitake, M.; Batina, N.; Itaya, K. *Langmuir* **1995**, *11*, 2337–2340.
(29) Batina, N.; Kunitake, M.; Itaya, K. *J. Electroanal. Chem.* **1996**, *405*, 245–250.
(30) Kunitake, M.; Akiba, U.; Batina, N.; Itaya, K. *Langmuir* **1997**, *13*, 1607–1615.
(31) Ogaki, K.; Batina, N.; Kunitake, M.; Itaya, K. *J. Phys. Chem.* **1996**, *100*, 7185–7190.
(32) Sashikata, K.; Sugata, T.; Sugimasa, M.; Itaya, K. *Langmuir* **1998**, *14*, 2896–2902.
(33) Wan, L. J.; Shundo, S.; Inukai, J.; Itaya, K. *Langmuir* **2000**, *16*, 2164–2168.
(34) Yoshimoto, S.; Inukai, J.; Tada, A.; Abe, T.; Morimoto, T.; Osuka, A.; Furuta, H.; Itaya, K. *J. Phys. Chem. B* **2004**, *108*, 1948–1954.
(35) Yoshimoto, S.; Tada, A.; Suto, K.; Narita, R.; Itaya, K. *Langmuir* **2003**, *19*, 672–677.
(36) Yoshimoto, S.; Sato, K.; Sugawara, S.; Chen, Y.; Ito, O.; Sawaguchi, T.; Niwa, O.; Itaya, K. *Langmuir* **2007**, *23*, 809–816.
(37) Yoshimoto, S.; Tsutsumi, E.; Suto, K.; Honda, Y.; Itaya, K. *Chem. Phys.* **2005**, *319*, 147–158.
(38) Yoshimoto, S.; Yokoo, N.; Fukuda, T.; Kobayashi, N.; Itaya, K. *Chem. Commun.* **2006**, 500–502.
(39) Yoshimoto, S.; Itaya, K. *J. Porphyrins Phthalocyanines* **2007**, *11*, 313–333.
(40) Tao, N. J.; Cardenas, G.; Cunha, F.; Shi, Z. *Langmuir* **1995**, *11*, 4445–4448.
(41) Tao, N. J. *Phys. Rev. Lett.* **1996**, *76*, 4066–4069.
(42) He, Y.; Ye, T.; Borguet, E. *J. Am. Chem. Soc.* **2002**, *124*, 11964–11970.
(43) Ye, T.; He, Y. F.; Borguet, E. *J. Phys. Chem. B* **2006**, *110*, 6141–6147.
(44) He, Y.; Borguet, E. *Angew. Chem., Int. Ed.* **2007**, *46*, 6098–6101.
(45) Neri, B. P.; Wilson, G. S. *Anal. Chem.* **1972**, *44*, 1002–1009.
(46) Wilson, G. S.; Neri, B. P. *Ann. N.Y. Acad. Sci.* **1973**, *206*, 568–578.

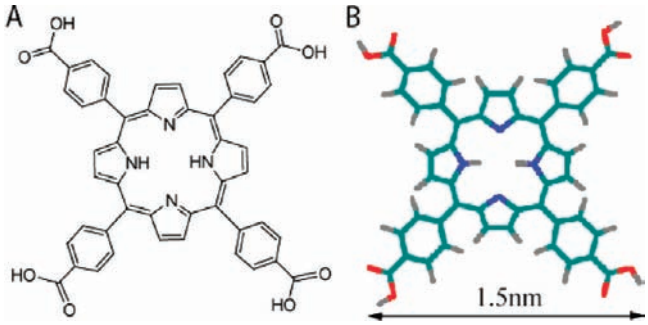

Figure 1. Chemical structure (A) and optimized model (B) (molecular mechanics, MM+) of TCPP molecules.

of TCPP; in other words, the slow reduction begins at a more positive potential than in the case of higher $[H^+]$.

Experimental Section

A single-crystal gold bead (attached to a gold foil) was used as substrate. Before each experiment, the substrate was cleaned by immersion in hot piranha solution (1:3 H_2O_2 (J. T. Baker, CMOS) and H_2SO_4 (J. T. Baker, CMOS) for 1 h (***Caution!*** *The piranha solution is a very strong oxidizing agent and extremely dangerous. Eye protection and gloves should be used during handling*), followed by rinsing and sonication in ultrapure water (>18 MΩ·cm, Barnstead, EasyPure system equipped with UV lamp). Finally, annealing in a hydrogen flame and cooling down in ambient atmosphere produced a bead where well-defined Au(111) facets with wide (>100 nm) terraces could be easily found.

TCPP was purchased from Frontier Scientific (Catalog No. T790, purity >97%) and used without further purification. Ethanol was used to dissolve TCPP because of its poor solubility in aqueous solution. Self-assembled layers were prepared by immersing the gold bead into a TCPP/ethanol (Alfa Aesar, Spectrophotometric grade) solution (10^{-5} M) for 2−3 min, rinsing thoroughly with ultrapure water, and then promptly mounting into a Teflon electrochemical cell containing $HClO_4$ (Fisher Scientific Co., trace metal grade) water solution under potential control (∼0.1 V). All potentials are quoted against saturated calomel electrode (SCE), though two platinum wires were used as counter and quasireference electrodes. All components (Teflon cell, O-ring, and ceramic tweezers) involved in the STM experiments were chemically cleaned in the same manner as the single-crystal gold bead. STM images were obtained with a PicoScan STM system (Molecular Imaging). STM tips were electrochemically etched (3 M KOH, ∼3−5 V) from tungsten wire (Alfa Aesar, 0.25 mm in diameter) and insulated with paraffin wax. The Faradaic current of the insulated tips under imaging conditions was typically less than 10 pA at experimental biases. All the STM images were obtained under constant current mode (0.5−0.7 nA) with a high-resolution scanner and without further processing (e.g., high-pass filtering) except necessary image flattening. Tunneling conditions are reported in the respective figure captions. Molecular models were built and optimized with Chemoffice Ultra 2006 software (CambridgeSoft, Inc.). The STM scan direction is upward, and estimated errors in the lattice parameters are 0.2 nm, unless further noted.

Results and Discussion

TCPP Self-Assembly Arrays. The chemical structure and optimized model of the TCPP molecule is shown in Figure 1. The molecular size (around 1.5 nm) was deduced with a simple molecular mechanics (MM+) calculation, and it is consistent with the reported EC-STM crystallographic data of ZnTCPP molecule.[47] STM imaging of TCPP layers was carried out in 0.01 M, 0.1 M, and 1 M $HClO_4$ solutions. A typical large scale STM image recorded in 0.01 M $HClO_4$ (Figure 2A) shows that adsorbed TCPP molecules formed an ordered self-assembly monolayer (SAM) on the Au(111) surface. Three different types of domains, marked by white labels, I, II, and III, are observed. Disordered boundaries separate the domains. These structures are stable and reproducible, extending over the atomically flat terrace of Au(111), indicating long-range order.

High-resolution STM images (Figure 2B−F) reveal the structural details of these three types of TCPP domains. TCPP molecules adopt a "flat-lying" orientation in all three cases. Domain type I is a highly ordered square packing TCPP network (Figure 2B), which is almost identical to the 3D crystallization structure of ZnTCPP,[47] with a trapped species inside the 2D network. This network structure is also similar to the STM results of carboxyl-substituted CoTCPP at Au(111)/0.1 M $HClO_4$ interfaces, in which a highly mobile "H_3O^+" was trapped in the void position of the square network.[38] The ordered adlayer structure is stable in the potential range of −0.2 V to +0.2 V. A few voids, possibly due to missing molecules, are occasionally observed as indicated by a white arrow in Figure 2B for an empty trap (void) site. A network structure with the same symmetry, but different contrast appearance, was also observed for an unknown reason in some experiments (Figure 2C). In this case the bright spots could be the trapped molecules of structure I. The trapped species are more likely to be individual TCPP molecules than highly mobile "H_3O^+" in this study because the inside and neighboring outside network molecules display a similar tunneling contrast in most images.[38] The unit cell lattice constant (black line in Figure 2G) is around 2.3 nm. A tentative structural model for domain type I is proposed based on Figure 2B and shown in Figure 2G. The TCPP molecules form a 2D network structure via hydrogen bonding (marked by black dotted ellipses in Figure 2G) between COOH groups from adjacent molecules and therefore adopt an orientation determined by the intermolecular hydrogen bonds between these groups. However, the orientation of void-trapped TCPP cannot be determined, possibly because of the rapid motion of the molecules.

A high resolution image (Figure 2D) of another ordered square packing TCPP network structure, labeled as domain type II in Figure 2A, shows a structure that is different from domain type I (Figure 2B,C). In domain type II, all the molecules are much closer to each other, forming a network without a vacancy void site. The intermolecular distance is around 1.8 nm. This structure is quite similar to the structure of TCPP domains when coadsorbed with stearic acid on HOPG, reported by Bai et al.[21] Most likely, hydrogen bonds via carboxyl groups also played an important role in this 4-fold symmetric square network structure. On the basis of this understanding, we propose an adsorption structural model shown in Figure 2H. The PhCOOH ring may or may not be coplanar with the porphyrin core, forming a hydrogen bond with the neighboring COOH groups of the adjacent TCPP molecules, as indicated by dotted black circles in Figure 2H.

In the domains shown in Figure 2E,F, the TCPP molecules form a hexagonal close-packing array (domain type III) with an intermolecular distance around 1.7 nm and an angle of ∼60° between adjacent molecular rows. These features are quite similar to the reported close-packing structures of TMPyP on I−Au(111) and CoP on the Au(111) surface.[28,34] In the former case, TMPyP molecules in adjacent molecular rows are rotated by 45° and extend one phenyl group into the vacancy between

(47) Diskin-Posner, Y.; Goldberg, I. *Chem. Commun.* **1999**, 1961–1962.

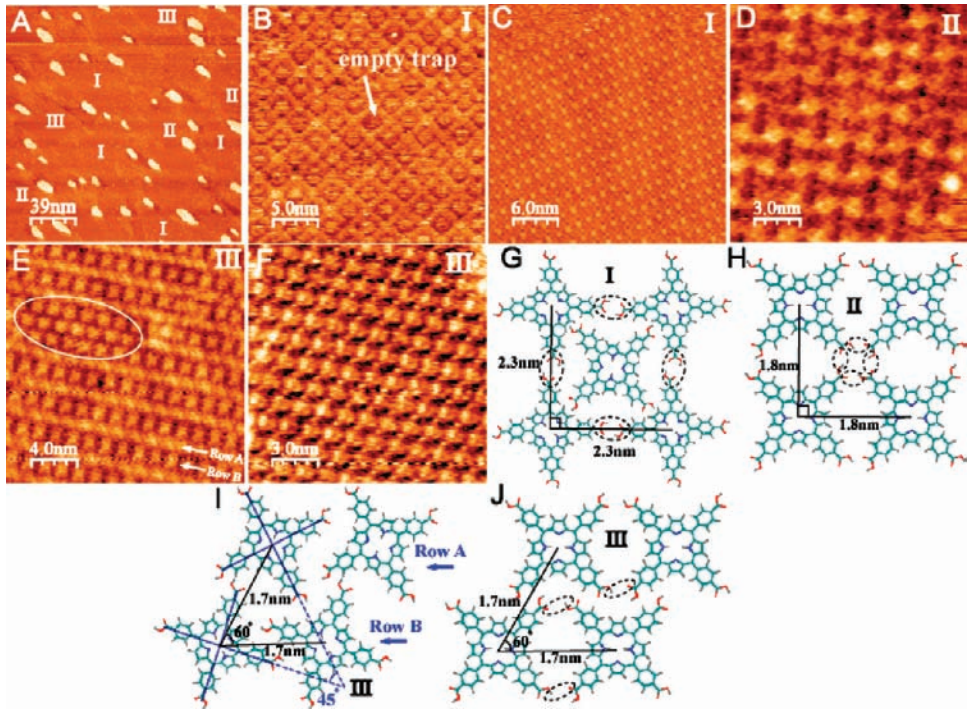

Figure 2. (A) Large scale STM image ($E = 0.15$ V, $E_{tip} \sim -0.03$ V, $I_{tip} \sim 0.6$ nA) of the self-assembled TCPP arrays on the Au(111) surface in 0.01 M $HClO_4$, revealing three types of domains marked by I, II, III. (B, C, D, E, and F) High resolution STM image ($E = 0.15$ V, $E_{tip} \sim -0.03$ V, $I_{tip} \sim 0.6$ nA) of the square network with and without the molecule trapped inside, to square packing and hexagonal close-packing arrays. (G, H, I, and J) Proposed structural models for the corresponding arrays.

two phenyl groups to form the 6-fold symmetry close-packing to minimize the surface free energy.[28] In the latter case, all molecules have a similar orientation on the surface.[34]

According to our STM images, these two types of adsorption features may coexist on the surface and even within the same domain sometimes (as marked by a white ellipse in Figure 2E). Therefore, we propose two types of models (Figure 2I,J) reflecting the possible arrangements for TCPP adsorption, although the reason for their coexistence in the same domain is unclear. In analogy with previous reports for TMPyP on I-Au(111),[28] we propose a structure (Figure 2I) where the relative orientation of TCPP in adjacent rows differs by ~45°, as marked by the blue line. We model the other arrangement seen in domain III by a structure (Figure 2J) where all the molecules have the same orientation, with possible hydrogen bonding between O and OH groups from neighboring molecules, as seen previously for CoP on Au(111).[34] It should be noted that the three adsorption arrays, domains I, II, and III, were observed in all the pH values studied.

TCPP Slow Reduction. The adsorption of porphyrins on an electrode surface may result in a loss or suppression in their electrochemical activities.[43,45,46,48] STM results provide direct evidence that surface adsorption affects adsorbate reduction.[43,44] After adsorption, the redox reaction of porphyrin is slowed down to the time scale of minutes, which can be observed at the single molecule level because the oxidized and reduced porphyrin molecules display different tunneling contrast in STM. This behavior provides an opportunity to investigate porphyrin electrochemistry at the molecular level.[43] Previous reports suggested that the first two-electron transfer happens after a protonation−deprotonation process between $P(0)H_4^{2+}$ and $P(0)H_2$ (as defined in Figure 8).[45,46] It is reasonable to expect that the $[H^+]$ should affect the porphyrin reduction channel, as it involves a protonation−deprotonation step.[45,46] However, the influence of $[H^+]$ on the slow reduction process after porphyrin adsorption is unknown, limiting our understanding of the mechanism of this redox reaction. The high resolution EC-STM studies of TCPP arrays in 0.01 M, 0.1 M, and 1 M $HClO_4$ solution described here provide, for the first time, information on the pH dependent porphyrin redox reaction at the electrochemical interface, revealing the reaction mechanism.

After successful observation of ordered adsorbate layers, the potential of the working electrode was stepped negative in 10 mV increments followed by several scans to check if any change in contrast, i.e., reduction, occurred. Our hypothesis was that contrast changes would be observable, because TCPP has a similar molecular structure to TPyP. During the scanning, all the TCPP molecules maintained the same tunneling contrast until a certain potential, negative enough to reduce the oxidized species, is reached. Interestingly, the reduction potential varies with the H^+ concentration of the supporting electrolyte. In images of TCPP arrays in 0.01 M $HClO_4$ right after the potential was stepped to 0.1 V (Figure 3A), it can be seen that some of the adsorbed TCPP molecules adopt a brighter contrast. A close inspection (Figure 3B) of the area circled by the white ellipse in Figure 3A indicates that the darks spots are not empty but actually contain molecules. We suggest that the brighter contrast molecules (highlighted by green boxes) correspond to reduced TCPP and that the darker species (highlighted by red boxes) are the oxidized form, consistent with our previous observation for the related molecule, TPyP.[43,44]

The slow reduction dynamics of TCPP at a potential of 0.1 V is shown in Figure 4 over the course of about 8 min. The number of brighter dots increases slowly from ~50 to ~150

(48) Bedioui, F.; Devynck, J.; Hinnen, C.; Rouseau, A.; Biedcharreton, C.; Gaudemer, A. *J. Electrochem. Soc.* **1985**, *132*, 2120–2124.

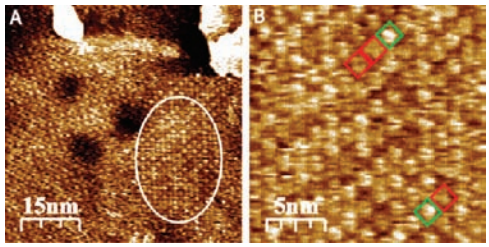

Figure 3. (A) TCPP arrays ($E = 0.1$ V, $E_{tip} \sim -0.05$ V, $I_{tip} \sim 0.6$ nA) in 0.01 M $HClO_4$ including a domain with brighter molecules inside a region marked by the white ellipse. (B) High resolution STM image ($E = 0.1$ V, $E_{tip} \sim -0.05$ V, $I_{tip} \sim 0.6$ nA) of the area enclosed in the white ellipse. Red box and green box represent the oxidized TCPP and reduced TCPP, respectively.

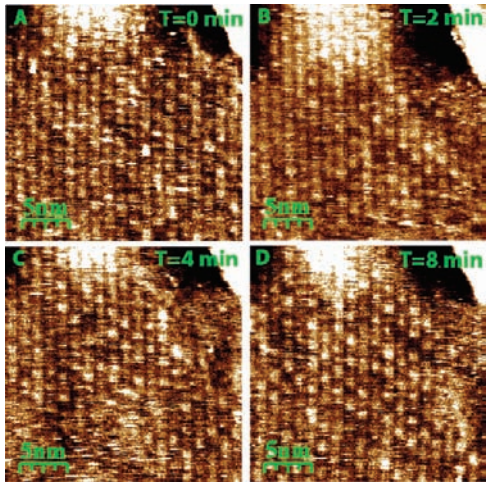

Figure 4. Slow reduction dynamics of TCPP after the potential was stepped from 0.12 to 0.1 V in 0.01 M $HClO_4$, ($E_{tip} \sim -0.03$ V, $I_{tip} \sim 0.6$ nA) revealed by an increasing number of brighter spots from A to D. (A) ~50 bright, (B) ~80, (C) ~100, (D) ~150. (All images scanned upward.)

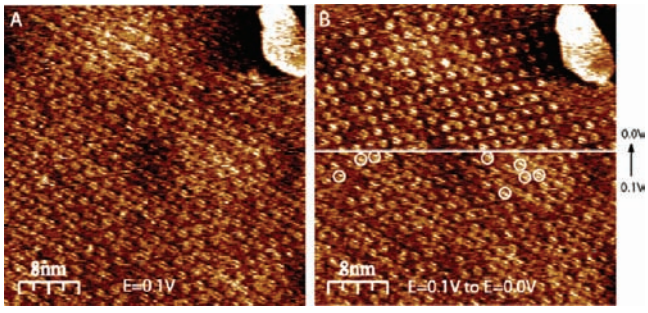

Figure 5. (A) TCPP arrays in 0.01 M $HClO_4$ at a potential of $E = 0.1$ V ($E_{tip} \sim -0.03$ V, $I_{tip} \sim 0.55$ nA) without any reduced molecules. (B) Image acquired after A. In the lower part of B, TCPP arrays at a potential of 0.1 V with only a few reduced TCPP (bright spots) marked by white circles are observed. In the upper part of B, most molecules in the TCPP array immediately become brighter after the potential change from 0.1 to 0.0 V in the middle of the image (marked by white line, $E_{tip} \sim -0.03$ V, $I_{tip} \sim$ 0.55 nA).

from Figure 4A−D. This reduction time scale is similar to that previously reported for TPyP.[43] When a more negative potential was used, e.g., 0.0 V, the slow reduction process immediately speeds up and brighter dots appear more quickly, as shown in Figure 5. At a potential of 0.1 V (Figure 5A), an area largely free of reduced TCPP was recorded. In the lower half of the subsequent upward scan, shown in Figure 5B, only a few TCPP molecules have been reduced (marked by white circles) because

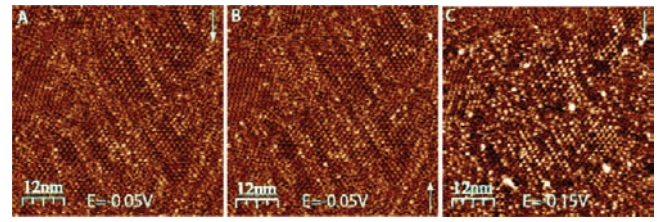

Figure 6. (A) TCPP arrays in 0.1 M $HClO_4$ at a potential of −0.05 V ($E_{tip} \sim -0.03$ V, $I_{tip} \sim 0.55$ nA) with several bright spots. (B) STM image after A, showing a slow increase of the number of bright spots at a potential of −0.05 V. (C) STM image after B: >50% of TCPP immediately become brighter after the potential was stepped to −0.15 V. Arrows indicate the scan directions. (The time separation between images is about 90 s.)

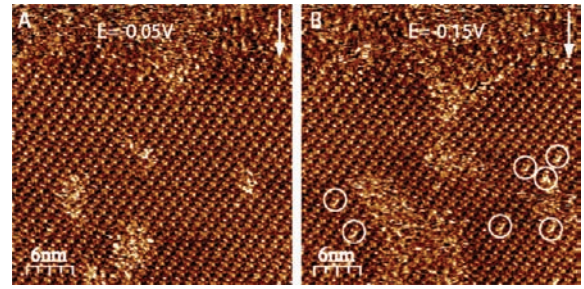

Figure 7. (A) TCPP arrays in 1 M $HClO_4$ at a potential of $E = -0.05$ V ($E_{tip} \sim -0.03$ V, $I_{tip} \sim 0.55$ nA) without bright spots. (B) STM image immediately after A, with several bright spots (marked by white circles) induced by a potential step to −0.15 V.

of the slow reduction rate at 0.1 V. After the substrate potential was suddenly changed to 0.0 V (marked by white line in Figure 5B, arrow indicates the scanning direction), at least 50% of the molecules immediately turned brighter in the rest upper part image, implying the formation of reduced TCPP. All TCPP molecules tend to turn brighter eventually as the experiment proceeds.

Experiments were also carried out in 0.1 M and 1 M $HClO_4$ solution in the same manner in order to investigate the $[H^+]$ influence on the reduction of TCPP arrays. Similar phenomena of slow surface reduction (at around −0.05 V) and acceleration of reduction (at around −0.15 V) were observed in 0.1 M $HClO_4$ as shown in a sequence of images of TCPP reduction (Figure 6A−C). However, a more negative initial reduction potential is needed to start the reduction process in 0.1 M compared to 0.01 M $HClO_4$. Here, the initial reduction potential is the potential at which slow reduction is observed, determined by the appearance of first several bright spots during slow scanning (~7 lines/s with a 512 × 512 image resolution). The reduction potential was ~0.15 V, more negative than the value in 0.01 M $HClO_4$. In other words, the reduction happens faster in 0.01 M $HClO_4$ than in 0.1 M $HClO_4$ at the same reduction potential. The same slow reduction process was observed in 1 M $HClO_4$ solution as well, with the initial reduction potential changed to even more negative value, around −0.15 V (Figure 7).

On the basis of the mechanism proposed by Wilson et al.,[46] there are two steps involving three porphyrin forms in this two-electron transfer process:

(1) A protonation and deprotonation reaction (PT) between two oxidized forms $P(0)H_2$ and $P(0)H_4^{2+}$ (as defined in Figure 8).

(2) An electron-transfer (ET) process between an oxidized form (either $P(0)H_4^{2+}$ or $P(0)H_2$) and a reduced form ($P(-II)H_4$).

The ET step can happen via two possible channels, either between $P(0)H_4^{2+}$ and $P(-II)H_4$ or between $P(0)H_2$ and $P(-II)H_4$,

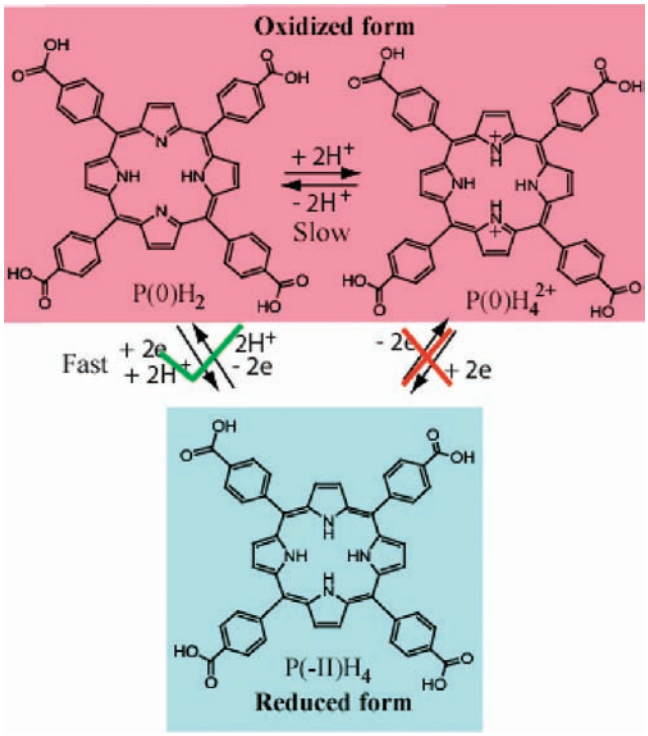

Figure 8. Proposed mechanism of TCPP reduction on Au(111) in an acidic medium. The protonated form of oxidized TCPP has suppressed electrochemical activity, so that reduction probably requires initial deprotonation.

depending on the H^+ concentration. Our EC-STM results indicate that the reduction of TCPP adsorbed on the Au surface is inhibited by higher $[H^+]$, which should promote the protonation process. In the acidic medium, the majority of oxidized species on the surface is likely to be the positively charged form, $P(0)H_4^{2+}$. In addition, the concentration of $P(0)H_4^{2+}$ should increase with an increasing $[H^+]$ (eqs 1 and 2), resulting in a decreased concentration of $P(0)H_2$.

$$P(0)H_4^{2+} \rightleftharpoons P(0)H_2 + 2H^+ \quad (1)$$

$$K = \frac{[P(0)H_2][H^+]^2}{[P(0)H_4^{2+}]} \quad (2)$$

Since the reduction slows down with increased $[H^+]$ concentration, which is likely due to the decreased concentration of active surface species, it is reasonable to suggest that $P(0)H_2$ is the active oxidized species in the reduction reaction pathway, i.e., TCPP is reduced from $P(0)H_2$ to $P(-II)H_4$ (eq 3).

$$P(0)H_2 + 2e^- + 2H^+ \rightleftharpoons P(-II)H_4 \quad (3)$$

Therefore, it appears that increasing $[H^+]$ converts the active species ($P(0)H_2$) to the inactive species ($P(0)H_4^{2+}$), slowing down the overall reduction rate.

To summarize the above discussion, we propose a model to describe the mechanism of the slow reduction of porphyrin molecules adsorbed on the electrode surface (Figure 8). In this model, the H^+ concentration does not influence the charge transfer reaction directly. Instead, it suppresses the reduction process by protonating the $P(0)H_2$ form of the porphyrin and turning it into $P(0)H_4^{2+}$, which has very limited electrochemical activity on the electrode surface. Although we propose that $P(0)H_4^{2+}$ does not react directly, it may be electrochemically reduced under other conditions that we did not explore. Alternatively, it may be reactive under the conditions in our experiments, but with a reaction rate much slower than the reduction of $P(0)H_2$. Our model is supported by the cyclic voltammetry (CV) results previously reported,[43] in which an initially oxidized porphyrin monolayer was stepped to a negative potential for various time durations, on the order of minutes, to reduce adsorbed porphyrins (Figure 2 in ref 43). Successive CV curves (Figure 3 in ref 43) show that the longer the holding time, the higher the redox peaks, clearly indicating a very slow reduction process. However, the CV curves themselves do not reflect the slow reduction because the reduction and oxidation peaks in each of the CV curve (Figure 3 in ref 43) have the same amplitude, revealing a reversible reaction scheme.

Our proposed model can explain this apparent contradiction easily. The observed slow reduction is an effect of $P(0)H_4^{2+}$ deprotonation, because the longer the holding time at negative potential, the more $P(0)H_4^{2+}$ is deprotonated to $P(0)H_2$, recovering the electrochemical activity of the reduced TPyP. The pH dependent experiments reported here provide additional information that enables us to refine the mechanism initially proposed (Scheme 2 in ref 43), in which the reduction reaction happened between $P(0)H_4^{2+}$ and $P(-II)H_4$. The reversible redox reaction observed in the CV curves is the fast reaction between $P(0)H_2$ and $P(-II)H_4$, which is reversible. It is also understandable that the reduction rate slows down at the longest holding times (asymptote of Figure 2 in ref 43) because the number of $P(0)H_4^{2+}$ that can be deprotonated decreases as the protonated, electrochemically inactive monolayer of $P(0)H_4^{2+}$ is depleted as the reaction proceeds.

Additional discussion should address which species correspond to the bright or dark spots we observed in EC-STM. It is clear that after reduction, the TCPP molecules turn bright, indicating that $P(-II)H_4$ are the bright spots in the STM images. Given the acidic condition during the experiments, most oxidized TCPP molecules are protonated. Therefore, the dominant features we observe at the beginning of reduction, i.e., dark spots, are the protonated form of oxidized TCPP, $P(0)H_4^{2+}$. However, it is not obvious whether the original form of oxidized TCPP ($P(0)H_2$) should be bright or dark. It is possible that $P(0)H_2$ turns bright right after deprotonating from $P(0)H_4^{2+}$ before the reduction takes place. In this case, bright spots represent both $P(0)H_2$ and $P(-II)H_4$ in STM images, while $P(0)H_4^{2+}$ is dark. In previous studies, it was reported that the oxidation of $P(-II)H_4$ is relatively fast compared to the reduction process.[44] It was shown that bright $P(-II)H_4$ changes to darker spots immediately after a short potential pulse, indicating that $P(0)H_2$ behaves as dark spots in STM images. Combining the present results and our previous reports, we conclude that both forms of the oxidized species ($P(0)H_2$ and $P(0)H_4^{2+}$) are the dark spots in STM images while the reduced form $P(-II)H_4$ is bright. Therefore our EC-STM observation of the contrast between bright and dark molecules in a TCPP monolayer is due to the different redox states of the molecules, i.e., the contrast is not introduced by the protonation/deprotonation process.

The observed slow reaction of TCPP is very similar to the reported TPyP redox reaction.[43,44] Taking into account that TCPP and TPyP share the same porphyrin core and that the overall geometry structure is very similar, it is reasonable to believe that the slow reduction takes place at the center of the porphyrin core, which supports the proposed model. We

hypothesize that this redox reaction mechanism can be generalized to other porphyrin molecules. Further investigation on a range of porphyrin molecules is needed to consolidate our knowledge of the redox reaction mechanism. It should be mentioned that the substitution groups in porphyrins may affect the redox reaction at the core. For example, TCPP is more acidic than TPyP, and the pyridyl groups of TPyP can easily undergo protonation and add positive charges to the overall molecule structure.

Conclusions

We demonstrate that tetracarboxylporphyrin (TCPP) forms three distinct types of ordered arrays on Au(111) in an acidic medium. Hydrogen bonding among the extended carboxyl groups of TCPP molecules appears to be the driving force for stable structure formation. TCPP molecules can be slowly reduced by tuning the potential of the underlying electrode. The more negative the potential, the faster the reduction rate of TCPP. Higher H^+ concentrations suppress the reduction process, indicating that the protonation of TCPP plays a negative role in the redox reaction. The EC-STM investigation of the pH dependent redox reaction of TCPP on the electrode surface is a critical piece to solve the puzzle of the porphyrin redox reaction mechanism at the electrochemical interface. On the basis of the experimental results, along with previously reported literature mechanisms, we proposed a new reaction model for the surface-adsorbed porphyrin molecules. This work provides evidence that the slow redox reaction takes place at the center of porphyrin core. In addition, the discovery of $[H^+]$ dependent reduction phenomena below pH = 2 extends, to lower pH, a reaction mechanism proposed in the literature.[45,46]

Acknowledgment. The authors acknowledge the generous support of the NSF (CHE0809838).

JA907397U